Effect of disorder on the electronic properties of graphene: A theoretical approach

Aftab Alam*
Division of Materials Science and Engineering, Ames Laboratory, Ames, Iowa 50011, USA

Biplab Sanyal
Department of Physics and Astronomy, Uppsala University, Box-516, 75120 Uppsala, Sweden

Abhijit Mookerjee
Department of Condensed Matter Physics and Materials Sciences, S. N. Bose National Centre for Basic Science, JD-III, Salt Lake City, Kolkata 700098, India

(Received 18 June 2012; published 29 August 2012)

In order to manipulate the properties of graphene, it is very important to understand the electronic structure in the presence of disorder. We investigate, within a tight-binding description, the effects of disorder in the on-site (diagonal disorder) term in the Hamiltonian as well as in the hopping integral (off-diagonal disorder) on the electronic dispersion and density of states by the augmented space recursion method. Extrinsic off-diagonal disorder is shown to have dramatic effects on the two-dimensional (2D) Dirac cone, including asymmetries in the band structures as well as the presence of discontinuous bands (because of resonances) in certain limits. Disorder-induced broadening, related to the scattering length (or lifetime) of Bloch electrons, is modified significantly with increasing strength of disorder. We propose that our methodology is suitable for the study of the effects of disorder in other 2D materials, such as a boron nitride monolayer.

DOI: 10.1103/PhysRevB.86.085454 PACS number(s): 73.22.Pr, 61.48.Gh

I. INTRODUCTION

Graphene, a two-dimensional allotrope of carbon, plays a central role in providing a basis for understanding the electronic properties of other carbon allotropes. Being one of the thinnest and the strongest material ever measured, graphene has attracted the attention of the materials research community[1] in the recent past. One of the most interesting aspects of graphene is that its low energy dispersion closely resembles the Dirac spectrum of massless fermions. This particular type of dispersion provides a bridge between condensed matter physics and quantum electrodynamics (QED) for massless fermions. Of course in graphene, the Dirac fermions move with a much smaller speed.

Because of its unusual electronic and structural flexibility, properties of graphene can be controlled chemically or structurally in many different ways, for example, by deposition of metal atoms[2] on top of the graphene sheet, incorporating other elements like boron and nitrogen[3] randomly in the parent structure, either interstitially or substitutionally and using different substrates.[4] Because disorder is unavoidable in any material, there has been an increasing interest in understanding how disorder affects the physics of electrons in graphene.[5] Disordered graphene based derivatives can probably be referred to as functionalized graphene suitable for specific applications. "*Graphene paper*"[6] is a spectacular example of how important such functionalization could be.

There can be many different sources of disorder in graphene including both intrinsic as well as extrinsic. Intrinsic sources may include surface ripples and topological defects. Extrinsic disorder comes in the form of vacancies, adatoms, quenched substitutional atoms, and extended defects, such as edges and cracks. Another way of introducing disorder is by ion irradiation that produces complex defect structures in the graphene lattice.[7] Graphene in an amorphous form may increase the metallicity too.[8]

To have a theoretical description of graphene's electronic structure, one may begin with the Kohn-Sham equation and a tight-binding representation whose basis is labeled by the sites of the underlying Bravais lattice. Disorder may enter the matrix representation of the Hamiltonian in two ways: vacancies, dopants, and adatoms predominantly cause a random change in the local single-site energy (disorder in the diagonal terms), but through the overlap such defects modify the hopping integrals between different sites (disorder in the off-diagonal terms) causing an effective random change in the distance or angle between the bonding orbitals. Thus diagonal and off-diagonal disorders simultaneously occur and are correlated. Model calculations which take them to be independent are qualitatively in error. As far as diagonal disorder is concerned, it acts as a simple chemical potential shift of the Dirac fermion, i.e., it shifts the Dirac point locally. Theoretical study of such disorder is rather simple and has indeed received attention and success, reported in the literature.[5–9] A proper inclusion of off-diagonal disorder, on the other hand, is nontrivial and requires more sophisticated approaches.

To date there have been numerous attempts at studying the effects of disorder in graphene.[5–9] Among others, the methods used to study effects of disorder included the averaged t-matrix approximation (ATA)[9] and the coherent potential approximation(CPA).[10] Several others have used exact diagonalization of huge clusters and the real-space recursion of Haydock *et al*.[9,11] Both these techniques actually calculate the density of states (DOS) for specific configurations of the system followed by direct averaging over a large number of configurations. Since each of the configurations has periodic boundary conditions, the averaged spectral function is always

a collection of δ functions and the disorder induced lifetime effects cannot be probed. The recursion on the lattice probes mainly the real-space effects of disorder.

From the theoretical perspective, dealing with disorder has had a long history. As mentioned earlier, one of the most successful and frequently used approaches is the single-site, mean field CPA.[10] However, as the name itself suggests, it is a single site approximation and cannot adequately take into account the effects of correlated configuration fluctuations. Among the hierarchy of the generalizations of the CPA, only few approaches proved promising and survived the test of time. These include the nonlocal CPA,[12] the special quasirandom structures (SQSs),[13] the locally self-consistent multiple scattering approach (LSMS),[14] and the three methods based on the augmented space formalism proposed by one of us:[15] the traveling cluster approximation (TCA),[16] the itinerant coherent potential approximation (ICPA),[17] and the augmented space recursion (ASR).[18] Over the years the ASR has proved to be one of the most powerful techniques, which can accurately take into account the effects of correlated fluctuations arising out of the disorder in the local environment. This is reflected in a series of studies in the past, e.g., the effects of local lattice distortion as in CuBe,[19] short-range ordering due to local chemistry,[20] the phonon problem[21] with essential off-diagonal disorder in the dynamical matrices, and electrical and thermal transport properties[22] in disordered alloys.

In this paper, we present a theoretical tight-binding model to study the effects of disorder in graphene. Disorders studied were mainly of two forms: substitutional disorder[23–25] and vacancies.[9,26] Unlike earlier models, both the diagonal and off-diagonal disorders are included on the same footing. The present formalism is based on the augmented space recursion.[18] Although recursion has been used to study graphene before, we want to emphasize that in *all* those applications recursion was carried out on a Hilbert space $\mathcal{H}$ spanned by the tight-binding basis representing the Hamiltonian. In augmented space recursion, we recurse in the space of all possible configurations which the Hamiltonian may assume in the disordered system. For a homogeneously disordered binary alloy, this configuration space is isomorphic to that of a spin-half Ising model. The augmented space theorem[15] then connects configuration averages to a specific matrix element in that space of configurations.

The novel approach in this work is that we shall make use of the translation symmetries in augmented space (for homogeneous disorder) to carry out recursion in reciprocal space. This will directly give us the spectral function from which we extract the "fuzzy" band structure. The inclusion of the effects of configuration fluctuations of the immediate environment gives us self-energies which are strongly **k** dependent, unlike the CPA. In order to make a systematic study, we present results for combinations of both strong and weak diagonal and off-diagonal disorder. The combined effects show dramatic changes in the location and topology of the Dirac-like dispersion and the DOS. Special emphasis has been given to the nontrivial inclusion of off-diagonal disorder, in which case the averaged Bloch spectral function comes out to be significantly broadened, multiply peaked, and asymmetric in certain limits where the presence of resonances leads to discontinuous dispersion. The interesting interplay of the two kinds of disorder on full widths at half maxima (FWHMs) (related to the lifetime of Bloch electrons in a disordered system) is also shown.

The rest of the paper is organized as follows. In Sec. II, we introduce the basic formalism. Section III is devoted to results and discussions. Concluding remarks are present in Sec. IV.

II. FORMALISM

The most general tight-binding Hamiltonian for electrons in graphene can be represented as

$$H = \sum_{R\alpha_s} \sum_{R'\alpha_{s'}} \{\epsilon_R^{\alpha_s} \delta_{RR'} \delta_{ss'} P_R^{\alpha_s} + V_{RR'}^{\alpha_s\alpha_{s'}} T_{RR'}^{\alpha_s\alpha_{s'}}\}, \qquad (1)$$

where R, R' denotes the position of the unit cell of the lattice, α_s denotes the αth atom on the sth sublattice. The actual atomic position is $R + \zeta^{\alpha_s}$, where ζ^{α_s} is the position of the αth atom on the sth sublattice. $\epsilon_R^{\alpha_s}$ is the on-site energy describing the

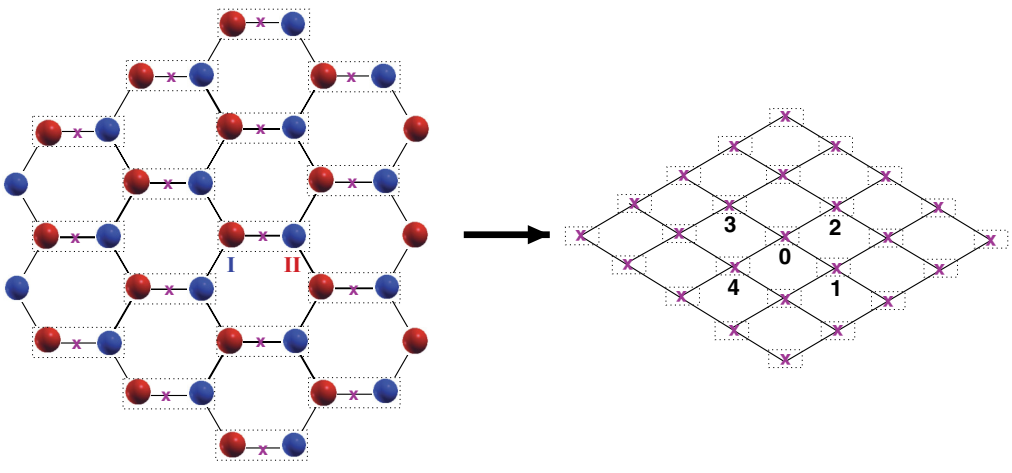

FIG. 1. (Color online) (Left) The standard honeycomb lattice with a basis of two atoms per unit cell. (Right) The underlying rhombic Bravais lattice which becomes the honeycomb lattice when a pair of atoms decorate each site.

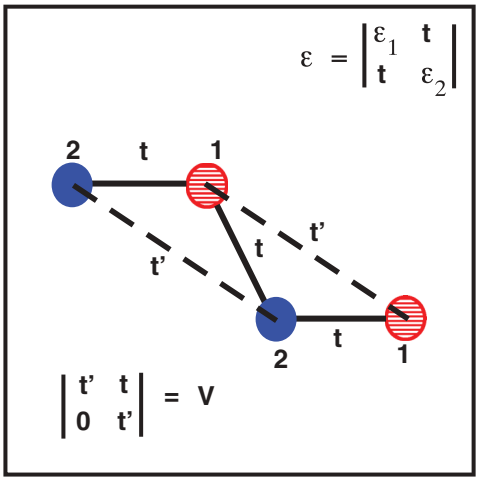

FIG. 2. (Color online) Nearest neighbor overlaps on the rhombic lattice.

scattering properties of the atomic potential at $R+\zeta^{\alpha_s}$, and $V_{RR'}^{\alpha_s\alpha_{s'}}$ is the hopping integral between $R+\zeta^{\alpha}$ and $R'+\zeta^{\alpha'}$. P and T are the projection and transfer operators in the Hilbert space spanned by the tight-binding basis $|R\alpha_s\rangle$.

The above Hamiltonian H describes electrons in the original honeycomb lattice of ion-cores, as shown in the left panel of Fig. 1. The two inequivalent sublattices (shown by red and blue spheres) are distinguished from each other. The underlying Bravais lattice is the rhombic lattice shown in the right panel of Fig. 1. Looking at Fig. 2 we can simplify Eq. (1) further and write the Hamiltonian elements as 2×2 matrices:

$$H=\sum_R \underline{\underline{\varepsilon}}_R\, P_R+\sum_{R\neq R'} \underline{\underline{V}}_{RR'} T_{RR'}, \tag{2}$$

where $\underline{\underline{\varepsilon}}_R$ and $\underline{\underline{V}}_{RR'}$, instead of being scalar for a single-band problem, are now 2×2 matrices given by

$$\begin{aligned}\underline{\underline{\varepsilon}}_R&=\begin{pmatrix}\epsilon_1 & t\\ t & \epsilon_2\end{pmatrix}\ \underline{\underline{V}}_{01}=\underline{\underline{V}}_{02}=\begin{pmatrix}t' & 0\\ t & t'\end{pmatrix},\\ \underline{\underline{V}}_{03}&=\underline{\underline{V}}_{04}=\begin{pmatrix}t' & t\\ 0 & t'\end{pmatrix},\end{aligned} \tag{3}$$

where ϵ_1 and ϵ_2 are the on-site energy on the two sublattices, and t and t' are the nearest neighbor and the next nearest neighbor hopping energies. $\underline{\underline{V}}_{0I}$ are the hopping matrices between the central site 0 and its four neighboring sites I (in the rhombic lattice) as shown in the right panel of Fig. 1. Because the next nearest neighbor hopping t' is usually very small compared to t, we shall treat the disorder effects only in the nearest neighbors.

For a system with substitutional disorder, the most general statement we can make is that the occupation of the lattice sites in each inequivalent sublattice can be different. For binary disorder in both the sublattices, we may introduce two random occupation variables n_R^I and n_R^{II} associated with the sublattices I and II such that,

$$n_R^I=\begin{cases}1 & \text{if}\quad R\in A \text{ with probability } x_A\\ 0 & \text{if}\quad R\in B \text{ with probability } x_B\end{cases}$$

and

$$n_R^{II}=\begin{cases}1 & \text{if}\quad R\in C \text{ with probability } x_C\\ 0 & \text{if}\quad R\in D \text{ with probability } x_D,\end{cases}$$

where A, B are the two types of atoms randomly occupying sublattice I and C, D are those occupying sublattice II.

The diagonal term $\underline{\varepsilon}_R$ for such a binary distribution can be written as

$$\begin{aligned}\underline{\varepsilon}_R&=\begin{pmatrix}\epsilon_A^I & t_{AC}\\ t_{AC} & \epsilon_C^{II}\end{pmatrix}n_R^I n_R^{II}+\begin{pmatrix}\epsilon_A^I & t_{AD}\\ t_{AD} & \epsilon_D^{II}\end{pmatrix}n_R^I(1-n_R^{II})\\ &+\begin{pmatrix}\epsilon_B^I & t_{BC}\\ t_{BC} & \epsilon_C^{II}\end{pmatrix}(1-n_R^I)n_R^{II}\\ &+\begin{pmatrix}\epsilon_B^I & t_{BD}\\ t_{BD} & \epsilon_D^{II}\end{pmatrix}(1-n_R^I)(1-n_R^{II})\\ &=E_1+E_2\,n_R^I+E_3\,n_R^{II}+E_4\,n_R^I n_R^{II},\end{aligned} \tag{4}$$

where

$$\begin{aligned}E_1&=\begin{pmatrix}\epsilon_B^I & t_{BD}\\ t_{BD} & \epsilon_B^{II}\end{pmatrix},\quad E_2=\begin{pmatrix}\delta\epsilon_1 & t^{(1)}\\ t^{(1)} & 0\end{pmatrix},\\ E_3&=\begin{pmatrix}0 & t^{(2)}\\ t^{(2)} & \delta\epsilon_2\end{pmatrix},\quad E_4=\begin{pmatrix}0 & t^{(3)}\\ t^{(3)} & 0\end{pmatrix},\end{aligned} \tag{5}$$

with $\delta\epsilon_1=\epsilon_A^I-\epsilon_B^I$; with $\delta\epsilon_2=\epsilon_C^{II}-\epsilon_D^{II}$; and with $t^{(1)}=t_{AD}-t_{BD}$, $t^{(2)}=t_{BC}-t_{BD}$, and $t^{(3)}=t_{AC}+t_{BD}-t_{AD}-t_{BC}$.

Similarly the off-diagonal term $\underline{V}_{RR'}$ in Eq. (3) can be expressed as (assuming $t'=0$)

$$\underline{V}_{01}=\underline{V}_{02}=V_1+V_2\,n_R^I+V_3\,n_{R'}^{II}+V_4\,n_R^I n_{R'}^{II}, \tag{6}$$

where

$$\begin{aligned}V_1&=\begin{pmatrix}0 & 0\\ t_{BD} & 0\end{pmatrix},\quad V_2=\begin{pmatrix}0 & 0\\ t^{(1)} & 0\end{pmatrix},\\ V_3&=\begin{pmatrix}0 & 0\\ t^{(2)} & 0\end{pmatrix},\quad V_4=\begin{pmatrix}0 & 0\\ t^{(3)} & 0\end{pmatrix}.\end{aligned} \tag{7}$$

$\underline{V}_{03}$ $(=\underline{V}_{04})$ are just the transpose of the above matrix $\underline{V}_{01}$. Various $t_{\alpha\beta}$'s in the above sets of equations are the hopping energies between various atom types ($\alpha=A,B$ and $\beta=C,D$) at two sublattices I and II, respectively.

Next we proceed to calculate the configuration averaged Green function (or the Bloch spectral function) in reciprocal space. We shall generalize the augmented space formalism (ASF) developed earlier in reciprocal space.[27] The ASF has been described in great detail earlier.[28] We shall indicate the main operational results here and refer the reader to the above monograph for further details. The first step is to associate with n_R^I and n_R^{II} two operators N_R^I and N_R^{II} such that their spectral density is the probability density of the random variables. For binary random variables, we have

$$N_R^I=\begin{pmatrix}x_B & \sqrt{x_A x_B}\\ \sqrt{x_A x_B} & x_A\end{pmatrix}.$$

Finally, according to augmented space theorem,[15] the configuration average of any function of $\{n_R^I,n_R^{II}\}$ can be written as the matrix element, in *configuration* space, of

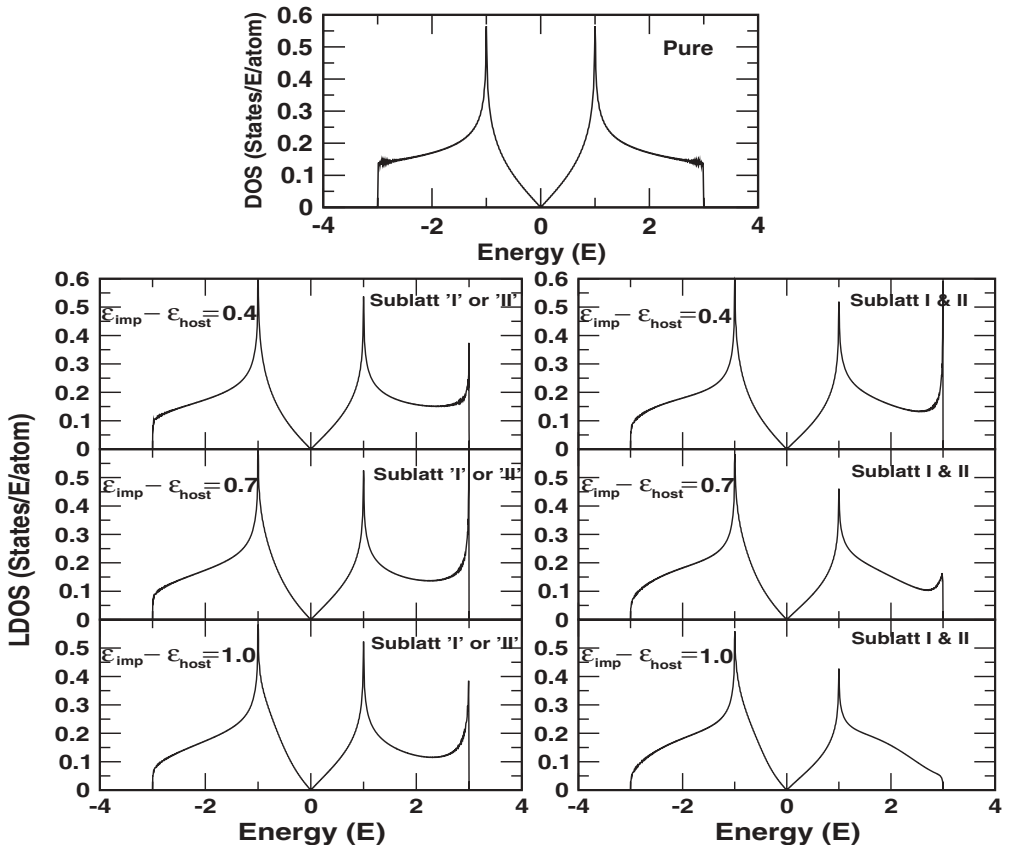

FIG. 3. Local density of states of pure graphene and graphene with a single or double impurity. The top panel in the middle is the DOS for pure graphene. Left panels show the local DOS at a sublattice I (or II) in the vicinity of an impurity site (single impurity). Right panels show the local DOS at a sublattice in the vicinity of an impurity site one of whose neighbors is also an impurity (double impurity). The panels from top to bottom are the results with increasing strength of the impurity potential $\delta E = \epsilon_{\rm imp} - \epsilon_{\rm host}$.

an operator which is the same functional of $\{N_R^I, N_R^{II}\}$. The augmented space Hamiltonian is built up from Eqs. (4) and (6):

$$\widehat{\mathbf{H}} = \sum_R \left\{E_1\widehat{I} + E_2\widetilde{N}_R^I + E_3\widetilde{N}_R^{II} + E_4\widetilde{N}_R^I \otimes \widetilde{N}_R^{II}\right\} \otimes P_R + \sum_R \sum_{R'} \left\{V_1\widehat{I} + V_2\widetilde{N}_R^I + V_3\widetilde{N}_{R'}^{II} + V_4\widetilde{N}_R^I \otimes \widetilde{N}_{R'}^{II}\right\} \otimes T_{RR'}$$

with

$$N_R^X = x_\alpha\, p_R^{X\uparrow} + x_\beta\, p_R^{X,\downarrow} + \sqrt{x_\alpha x_\beta}\left(\tau_R^{X,\uparrow\downarrow} + \tau_R^{X,\downarrow\uparrow}\right), \quad (8)$$

(X = I or II).

The configuration averaged Green's function in the reciprocal space is thus a matrix element of an augmented resolvent given by

$$\langle\langle G(\mathbf{k},z)\rangle\rangle = \langle\{\emptyset\}\otimes\mathbf{k}|(z\widehat{\mathbf{I}} - \widehat{\mathbf{H}})^{-1}|\,\mathbf{k}\otimes\{\emptyset\}\rangle, \quad (9)$$

$|\mathbf{k}\otimes\{\emptyset\}\rangle$ is an augmented space state in the reciprocal space given by

$$|\mathbf{k}\otimes\{\emptyset\}\rangle = \frac{1}{\sqrt{N}}\sum_R e^{-i\mathbf{k}.\mathbf{R}}|R\otimes\{\emptyset\}\rangle, \quad (10)$$

and $|R\otimes\{\emptyset\}\rangle$ is an enlarged basis which is a direct product of the Hilbert space basis $\{R\}$ and the configuration space basis $\{\phi_R\}$. The configuration space $\Phi = \prod_R^{\otimes}\phi_R$, which takes care of the statistical average, is of rank 2^M for a system of M-lattice sites with binary distribution.

The recursion follows as a three step generation of a new basis $\{|n>\}$:

$$|1\rangle = |\mathbf{k}\otimes\{\emptyset\}\rangle, \quad |0\rangle = 0,$$
$$|n+1\rangle = \widehat{H}|n\rangle - \alpha_n|n\rangle - \beta_{n-1}^2|n-1\rangle,$$
$$\alpha_n(\mathbf{k}) = \frac{\langle n|\widehat{H}|n\rangle}{\langle n|n\rangle} \quad \text{and} \quad \beta_n^2(\mathbf{k}) = \frac{\langle\mathbf{n}|\mathbf{n}\rangle}{\langle\mathbf{n}-\mathbf{1}|\mathbf{n}-\mathbf{1}\rangle}.$$

The ASR gives the configuration averaged spectral function as a continued fraction:

$$\langle\langle G(\mathbf{k},z)\rangle\rangle = \cfrac{1}{z-\alpha_1(\mathbf{k}) - \cfrac{\beta_1^2(\mathbf{k})}{z-\alpha_2(\mathbf{k}) - \cfrac{\beta_1^2(\mathbf{k})}{z-\alpha_3(\mathbf{k}) - \cfrac{\ddots}{T(z,\mathbf{k})}}}} = \frac{1}{z - E_0(\mathbf{k}) - \Sigma(z,\mathbf{k})}. \quad (11)$$

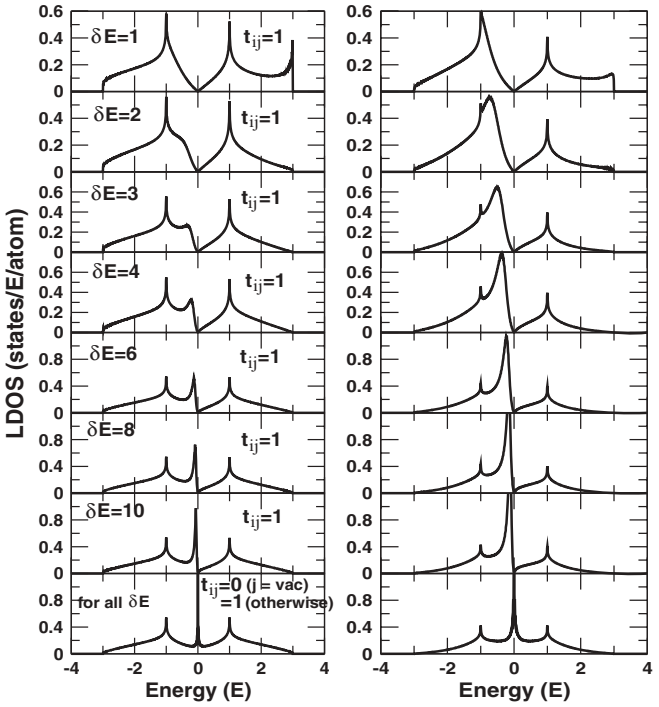

FIG. 4. Local DOS at a particular sublattice in the vicinity of a single (left panels) or double (right panels) vacancy site in graphene. A vacancy site is modeled by a site with a large repulsive local potential. Technically we take $\delta E = \epsilon_{\rm imp} - \epsilon_{\rm host}$ for both the single and double impurity problems. The figures show consecutive situations with increasing δE as we go from top to bottom. The very bottom panels indicate the ideal case of a completely inaccessible *hard* vacancy with $t_{ij} = 0$.

$T(z,\mathbf{k})$ is a continued fraction *terminator* as proposed by Beer and Pettifor.[29] The spectral function peaks are decided by $\Re e\{\Sigma(E,\mathbf{k})\}$, and the imaginary part of Σ gives the width related to the disorder induced lifetimes.

The configuration averaged Bloch spectral function is given by

$$\langle\langle A(\mathbf{k},E)\rangle\rangle = -\frac{1}{\pi}\lim_{\delta\to 0^+}\Im m\{\langle\langle G(\mathbf{k},E+i\delta)\rangle\rangle\}. \qquad (12)$$

The configuration averaged DOS is

$$\langle\langle n(E)\rangle\rangle = \frac{1}{\Omega_{BZ}}\int_{BZ} d\mathbf{k}\,\langle\langle A(\mathbf{k},E)\rangle\rangle. \qquad (13)$$

The electronic dispersion curves are obtained by numerically calculating the peak E position of the spectral function. The FWHMs are also calculated from the disorder broadened Bloch spectral function.

III. RESULTS AND DISCUSSION

In the following subsections, we shall present our results for graphene with impurities, vacancies, diagonal disorder alone, and with the simultaneous presence of diagonal and off-diagonal disorder. The effects of various strengths of impurity potentials on two inequivalent sublattices will be shown via changes in the shape of the DOS. The changes

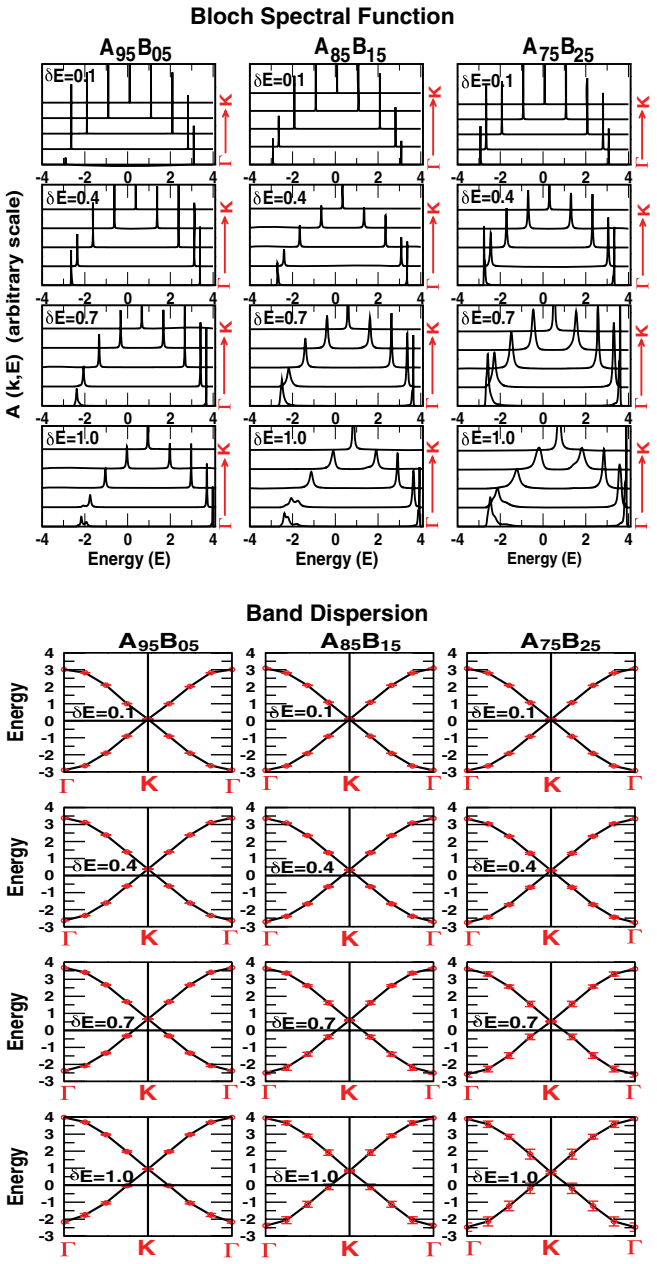

FIG. 5. (Color online) Configuration averaged spectral functions (upper set of panels) and the complex dispersion (lower set of panels) near the Dirac point. These are all for pure diagonal disorder at three different alloy compositions (left to right) and four disorder strengths δE (top to bottom). The (red) error bars show how the disorder induced lifetimes vary across the samples.

in the topology of Dirac-cone dispersion, disorder-induced FWHMs, and the DOS will be shown for various strengths of diagonal disorder. In the most general case of diagonal and off-diagonal disorder, we consider three interesting limiting cases: (i) strong diagonal and weak off-diagonal disorder, (ii) strong off-diagonal and weak diagonal disorder, and (iii) strong diagonal as well as off-diagonal disorder. The interesting interplay between these different kinds of disorder in graphene reveals a discontinuous type of band near the Γ point in the third limiting case.

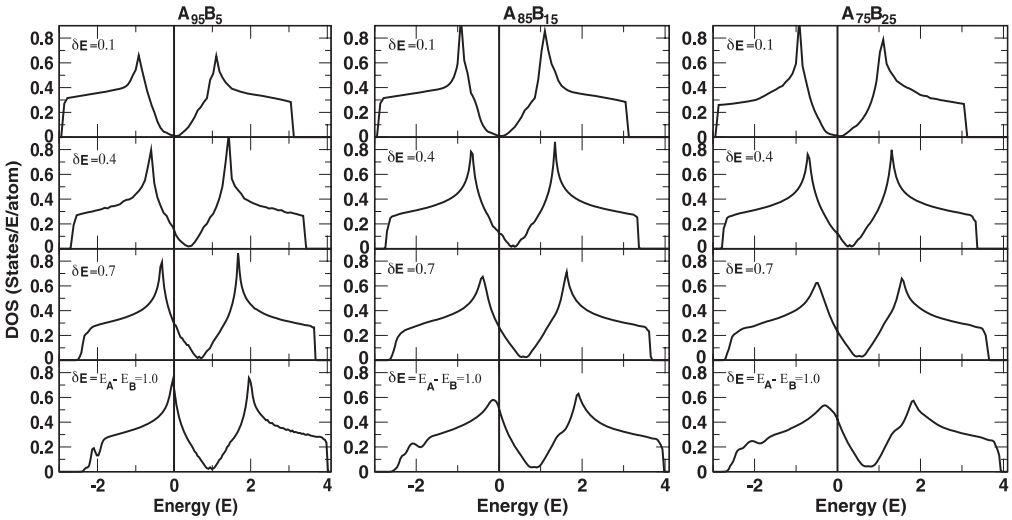

FIG. 6. Total DOS for the same set of disorder strengths δE for the three alloys $A_{x_A}B_{x_B}$ as in Fig. 5. Due to homogeneous diagonal disorder on both the sublattices I and II, the individual projected DOSs on them are same in this case.

A. Impurities in Graphene

In Fig. 3, we display the local DOS with different strengths of the single and double impurity potentials on different inequivalent sublattices. The top figure in the middle panel is the DOS for pure graphene. Left panels show the local DOS at a sublattice (I or II) in the vicinity of an impurity site, while right panels show the local DOS in the vicinity of an impurity site one of whose neighbors is also an impurity with the same potential (i.e., a double impurity, one at sublattice I and the other at II). The strength of the impurity potential (relative to the host lattice) increases from top to bottom panels (i.e., $\delta E = \epsilon_{\text{imp}} - \epsilon_{\text{host}} = 0.4$, 0.7, and 1.0). All these calculations are done with a fixed hopping parameter $t = 1$. We notice changes in the shape of the hump and the van Hove singularities as the strength of the impurity potential increases. Although the effects are small, they are clearly visible for the case of $\delta E = 1.0$, where the local environment around the impurity site feels the strongest scattering. With the introduction of the impurity, the symmetry of the DOS around the Dirac point is lost. At these impurity levels, both the left and right panels show the formation of an impurity peak near the upper band edge. With increasing disorder this impurity peak moves into the band and disappears. Again, at these strengths there is no perceptible changes to the linear structure of the Dirac point. Similar results have been obtained previously for such models of impurities. This provides the correctness of our new formulation.

B. Single vacancies in graphene

Let us now extend the impurity problem to the vacancies. A vacancy can be modeled by a site with a large repulsive local potential. Figure 4 shows the results for a single and double vacancy. Left (right) panels show the local density of states (LDOS) at a central site located in the vicinity of a single (double) impurity site(s). A single vacancy corresponds to just one nearest-neighbor (NN) impurity site while a double vacancy to two NN sites around the central site at which the LDOS is projected. Top to bottom panels indicate the evolution of the structure of the DOS with increasing strength of the local potential (δE) at the impurity site(s). The panels at the very bottom show the results for the case of the ideal vacancy, where $t_{ij} = 0$ for t connecting the vacancy site to the graphene lattice, or in other words a completely inaccessible "hard" vacancy. Notice that, with increasing δE, the right-most impurity peak at around the top band edge moves into the band. Most of the changes occur around the Dirac point at $E = 0$. With the introduction of impurity, the symmetry of the DOS around the Dirac point gets broken and an extra impurity peak starts to appear near $E = 0$ (for $\delta E \geqslant 2$). The origin of such a "zero mode" resonant peak has been discussed in detail by Pereira *et al.*[30] and Wehling *et al.*[25] This peak grows in height with increasing potential strength and decreases in width.

As observed by Wehling *et al.*,[25] we also noticed a similar impurity resonance peak within $E = 1$ eV (with varying potential strength) around the Dirac point. Such a resonance peak structure is located further away from $E = 0$ for weaker impurity potentials, and moves towards $E = 0$ with increasing scattering strength. Single and double impurity cases do reflect different electronic effects on the projected LDOS. In the case of double impurity, the resonance peak is broadened (due to more scattering) and lies further away from $E = 0$ as compared to the single impurity case. The evolution of the impurity peak and the symmetry of the DOS on the two sides of Dirac point are much more sensitive to the change of scattering strength in the double impurity case. The structure of the DOS changes more dramatically in the weaker potential regime. Symmetry of the LDOS on the two sides of the Dirac point ($E = 0$) starts to reform more quickly with the strength of the potential in the case of a single impurity than the double ones. Eventually, in the case of a hard-wall impurity (ideal vacancy), the sharp resonance peak appears perfectly at the Dirac point ($E = 0$) and the symmetry of the DOS around $E = 0$ is completely restored.

C. Diagonal disorder

First we shall take up purely diagonal disorder problems: those problems which can be taken up by earlier suggested

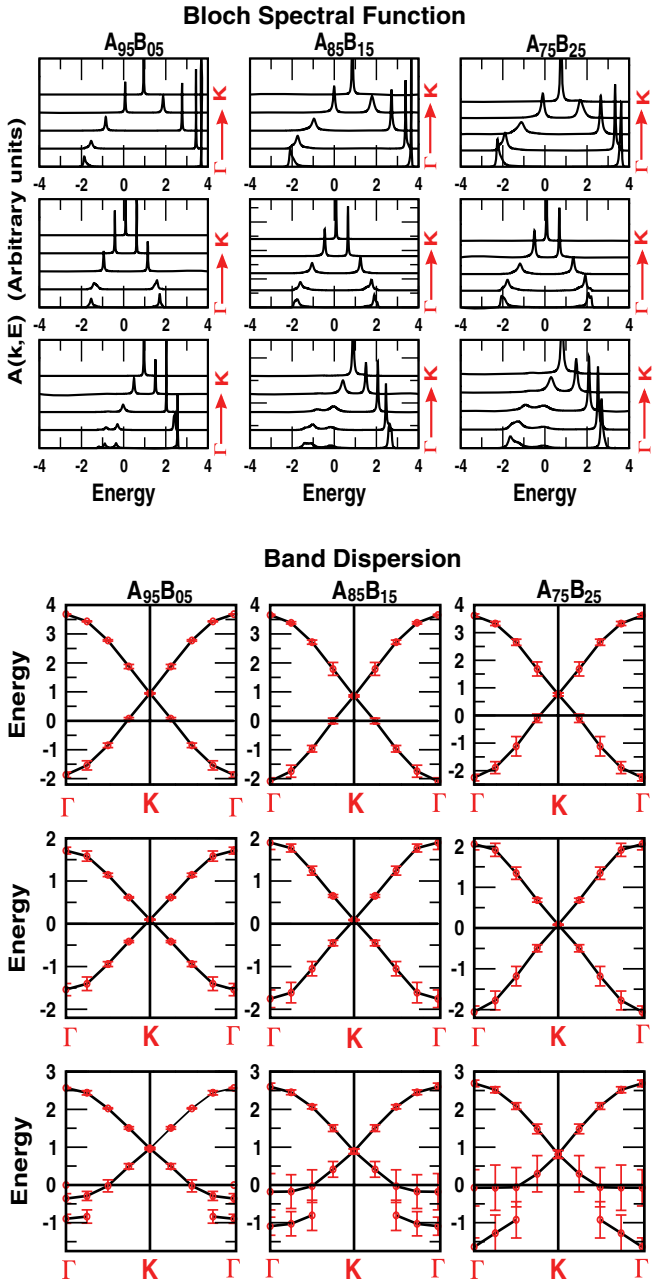

FIG. 7. (Color online) Same as Fig. 5, but with the inclusion of both diagonal and off-diagonal disorder. The three panels for each alloy indicate the results with coupled diagonal and off-diagonal disorders as described in the text.

methodologies. Of course, our augmented space recursion in reciprocal space gives us additional information about the disorder induced lifetimes of the Bloch states. In Fig. 5, we display the configuration averaged Bloch spectral function (upper panels) [given by Eq. (12)] and the corresponding dispersion energy vs k (lower panels) along the Γ-K-Γ symmetry line for three different alloys $A_{x_A}B_{x_B}$ ($x_B = 5\%, 15\%$, and 25%) with various diagonal disorder strengths. For each disorder strength δE in a particular alloy, the upper panels show the averaged Bloch spectral function at five $\mathbf{k}$ points along the high symmetry direction Γ-K. The corresponding Dirac dispersions are shown in the lower set of panels along the Γ-K-Γ line. The two sublattices I and II are homogeneously disordered, such that $x_A = x_C$, $x_B = x_D$ and $\epsilon_A^I = \epsilon_C^{II}$, $\epsilon_B^I = \epsilon_D^{II}$. For each alloy case, the panels from top to bottom indicate the results with increasing strength of diagonal disorder (i.e., $\delta E = \epsilon_A - \epsilon_B = 0.1, 0.4, 0.7$, and 1.0). The hopping integral t is chosen to be 1 here, so there is no off-diagonal disorder. The first thing to note is that the spectral function modifies quickly from sharp near δ functions to Lorentzian shapes with increasing disorder strength δE as well as increasing alloy concentration x_B. In addition, the function gets more and more asymmetric with increasing δE. Such asymmetries can be described as a tendency of more scattering to occur near the resonance energies around Γ. In other words, line shapes around Γ tend to have a weak second peak or wide tail over the resonance region. For the present diagonal disordered case, the Dirac point is simply shifted by an average energy $\langle\epsilon\rangle = x_A\epsilon_A^I + x_B\epsilon_B^{II}$.

The corresponding total DOS for the same set of disorder strengths δE and the alloy concentrations x are shown in Fig. 6. The individual projected DOS on the two sublattices I and II in this case are same, because we have maintained uniform diagonal disorder on both the sublattices. However, the present theory is equally capable of treating the two sublattices differently with a different nature of disorder on them. In that case, the two inequivalent sublattices will have different projected quantities. Looking at Fig. 6, one can notice an exactly similar shift of the Dirac point (to the average $\langle\epsilon\rangle$) in the DOS as shown in the dispersion. The disorder effects are pronounced around the Dirac-point energy $\langle\epsilon\rangle$ and get milder around the hump below $\delta E = 0.7$. Above this disorder strength, the left band edge starts to show up extra features with a dip at around $E = -2$ (as shown in the bottom panels for the three alloy concentrations). The results are qualitatively similar to the CPA works done earlier[30] but differ in quantitative details.

D. Off-diagonal disorder

We now turn to the cases with off-diagonal disorder. Such problems cannot be dealt with within the CPA. Also, direct calculation of the averaged spectral functions and disorder induced lifetimes is also not feasible with other techniques and the strength of the ASR comes to the fore. In addition we should note that in our model, diagonal and off-diagonal disorders are correlated: e.g., if the atom A occupies the site i with probability x_A and atom B occupies the site j with probability x_B, then t_{ij} *has to be* t_{AB} with probability 1. Although the present theory is equally capable of investigating other interesting cases (e.g., inhomogeneous disorder, pseudobinary type disorder, etc.), here we have chosen to explore three cases which should reflect the behavior of a variety of the realistic materials. The three cases are

(i) strong diagonal and weak off-diagonal disorder with parameters $\delta E = \epsilon_A^I - \epsilon_B^I = \epsilon_C^{II} - \epsilon_D^{II} = 1.0$, $t_{AC} = 1.0$, $t_{BD} = 0.9$, and $t_{AD} = t_{BC} = 0.95$;

(ii) weak diagonal and strong off-diagonal disorder with parameters $\delta E = 0.1$, $t_{AC} = 1.0$, $t_{BD} = 0.5$, and $t_{AD} = t_{BC} = 0.75$; and

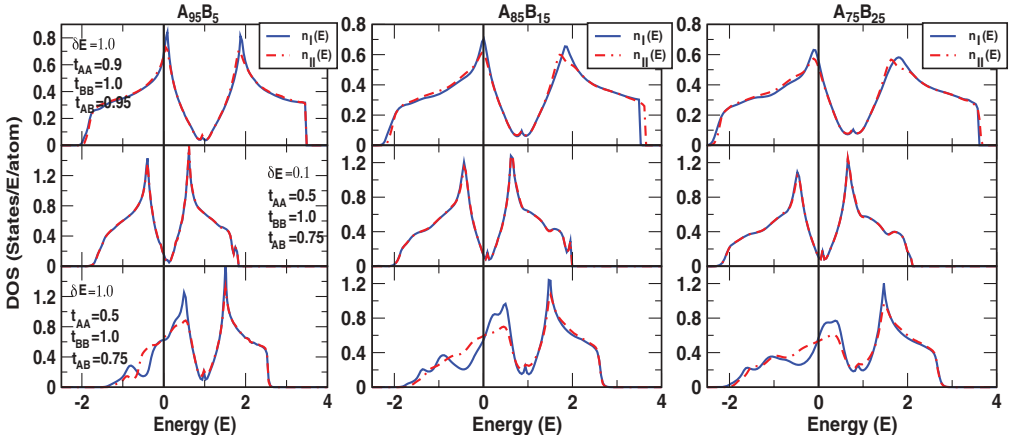

FIG. 8. (Color online) Sublattice projected DOS for the same three sets of diagonal + off-diagonal disorder strengths for three alloys $A_{x_A}B_{x_B}$ as in Fig. 7. The projected DOSs on the two sublattices n_I and n_{II}, in this case, are different due to the obvious reason arising from different random t_{ij} interactions.

(iii) strong diagonal as well as strong off-diagonal disorder with parameters $\delta E = 1.0$, $t_{AC} = 1.0$, $t_{BD} = 0.5$, and $t_{AD} = t_{BC} = 0.75$.

The results for these three cases are shown in the top, middle, and bottom panels of Fig. 7, respectively, for the same three alloys $A_{x_A}B_{x_B}$ as before. Other details are same as in Fig. 5. Notice that unlike the diagonal disordered case, effects of both diagonal and off-diagonal disorder are much more dramatic. In addition to a highly asymmetric nature, the Bloch spectral function is found to have a double peaked structure in the extreme case of strong diagonal and off-diagonal disorder (shown in the bottom panels). Such a doubly peaked line shape introduces extra discontinuous bands in the dispersion curve. Such a structure had been seen before in phonon problems[21] which also have intrinsic off-diagonal disorder in the dynamical matrices. There it arose because of resonant modes. Here too we shall give a similar explanation. These dispersions at resonance have relatively large FWHMs, and it will be interesting to choose a realistic material of similar disorder properties and investigate the experimental outcome.

Figure 8 shows the sublattice projected DOS for the same three limiting cases for the three alloys as above. The solid blue and the dashed red lines indicate the projected DOSs on the sublattices I and II, respectively. Because of the random hopping (off-diagonal) interaction in this case, the two sublattices acquire a different environment around it, and hence possess different projected quantities on them. As expected, the DOSs in these cases have large smearings. The effective environment around the two sublattices is maximally different from each other in the extreme case of both strong diagonal + off-diagonal disorders (as shown in the bottom panels), as evident from the large difference between their projected DOSs. Interestingly, for this particular case, the appearance of discontinuous bands in the -ve energy range (see bottom panels of Fig. 7) is reflected via a dip in the DOS along with a much larger smearing. Apart from this extreme case, the Dirac point for all the other cases has moved in exact accordance with that of the band shift as in Fig. 7. The topology of the DOS on the two sides of the Dirac point are very different from each other especially in the case of strong diagonal and off-diagonal disorder (bottom panels). In totality, the effects of off-diagonal disorder are very different from that of diagonal disorder (as a comparison between Figs. 6 and 8 will show). Treatments of off-diagonal disorder is straightforward and accurate in the ASR formalism.

IV. CONCLUSION

We present a theoretical model to study the effects of (i) impurities and (ii) substitutional diagonal and off-diagonal disorder in graphene on an equal footing. Local electronic properties of impurity (single and double) states are found to agree fairly well with other theoretical approaches and are open to connect with the future scanning tunneling spectroscopy (STS) experiments which are capable of extracting a local density of states which can be directly compared with our results. Moreover,our calculated band dispersions can be compared with angle-resolved photoemission experiments, which have been done for ordered graphene by several groups. In regards to substitutional disorder, we show how the topology of the Dirac dispersion and the location of the Dirac point change with the strength of disorder. We reliably take into account the effects of off-diagonal disorder in describing the spectral properties of graphene. The present approach is based on a model Hamiltonian with varying diagonal and off-diagonal disorder strengths. Our main aim was to provide the trend for the electronic dispersion, DOS, and the disorder-induced scattering with various combination of disorder, which in fact should help in understanding the electronic properties of realistic graphene materials with similar types of disorder. One of our interesting findings is the dispersion in the case of both strong diagonal and off-diagonal disorder which tends to have an extra discontinuous band: a rather uncommon feature in the graphene fermiology with simple disorder. As such we propose to verify such effects in the electronic dispersion by setting up an experiment on a realistic graphene system, where both the diagonal and the off-diagonal disorder are strong (e.g., creating a disordered graphene structure with a variety of structural defects introduced by ion irradiation and then

adsorbing transition metal adatoms or clusters at some defect sites as the chemisorption energy is very high at the defect sites[31]). We believe that such a study may provide a deeper insight into the physics and materials perspective of graphene. Finally, we want to state that our formulation is quite general and can be applied to any realistic two dimensional (2D) material, e.g., BN in the presence of disorder.

ACKNOWLEDGMENTS

A.A. acknowledges support from the U.S. Department of Energy BES/Materials Science and Engineering Division from Contract No. DEFG02-03ER46026 and Ames Laboratory (Contract No. DE-AC02-07CH11358), operated by Iowa State University. This work was done under the HYDRA Collaboration between the research groups.

*aftab@ameslab.gov

[1] A. H. Castro Neto, F. Guinea, N. M. R. Peres, K. S. Novoselov, and A. K. Geim, Rev. Mod. Phys. **81**, 109 (2009).

[2] M. Calandra and F. Mauri, Phys. Rev. B **76**, 161406 (2007); **76**, 199901(E) (2007); B. Uchoa, C. Y. Lin, and A. H. Castro Neto, *ibid.* **77**, 035420 (2008).

[3] T. B. Martins, R. H. Miwa, A. J. R. da Silva, and A. Fazzio, Phys. Rev. Lett. **98**, 196803 (2007).

[4] I. Calizo, W. Bao, F. Miao, C. N. Lau, and A. A. Balandin, Appl. Phys. Lett. **91**, 201904 (2007); G. Giovannetti, P. A. Khomyakov, G. Brocks, P. J. Kelly, and J. van den Brink, Phys. Rev. B **76**, 073103 (2007).

[5] V. A. Coleman, R. Knut, O. Karis, H. Grennberg, U. Jansson, R. Quinlan, B. C. Holloway, B. Sanyal, and O. Eriksson, J. Phys. D: Appl. Phys. **41**, 062001 (2008); S. H. M. Jafri, K. Carva, E. Widenkvist, T. Blom, B. Sanyal, J. Fransson, O. Eriksson, U. Jansson, H. Grennberg, O. Karis, R. A. Quinlan, B. C. Holloway, and K. Leifer, *ibid.* **43**, 045404 (2010); K. Carva, B. Sanyal, J. Fransson, and O. Eriksson, Phys. Rev. B **81**, 245405 (2010).

[6] D. A. Dikin *et al*., Nature (London) **448**, 457 (2007).

[7] F. Banhart, J. Kotakoski, and A. V. Krasheninnikov, ACS Nano **5**, 26 (2011).

[8] E. Holmström, J. Fransson, O. Eriksson, R. Lizarraga, B. Sanyal, S. Bhandary, and M. I. Katsnelson, Phys. Rev. B **84**, 205414 (2011).

[9] Shangduan Wu, Lei Jing, Qunxiang Li, Q. W. Shi, Jie Chen, Haibin Su, Xiaoping Wang, and Jinlong Yang, Phys. Rev. B **77**, 195411 (2008).

[10] P. Soven, Phys. Rev. **156**, 809 (1967); G. M. Stocks, W. M. Temmerman, and B. L. Gyorffy, Phys. Rev. Lett. **41**, 339 (1978).

[11] R. Haydock, V. Heine, and M. J. Kelly, J. Phys. C: Solid State Phys. **5**, 2845 (1975).

[12] D. A. Biava, Subhradip Ghosh, D. D. Johnson, W. A. Shelton, and A. V. Smirnov, Phys. Rev. B **72**, 113105 (2005); Derwyn A. Rowlands, Julie B. Staunton, Balazs L. Györffy, Ezio Bruno, and Beniamino Ginatempo, *ibid.* **72**, 045101 (2005).

[13] A. Zunger, S. H. Wei, L. G. Ferreira, and J. E. Bernard, Phys. Rev. Lett. **65**, 353 (1990).

[14] Y. Wang, G. M. Stocks, W. A. Shelton, D. M. C. Nicholson, Z. Szotek, and W. M. Temmerman, Phys. Rev. Lett. **75**, 2867 (1995).

[15] Abhijit Mookerjee, J. Phys. C: Solid State Phys. **6**, L205 (1973).

[16] R. Mills and P. Ratanavararaksa, Phys. Rev. B **18**, 5291 (1978); T. Kaplan, P. L. Leath, L. J. Gray, and H. W. Diehl, *ibid.* **21**, 4230 (1980).

[17] S. Ghosh, P. L. Leath, and M. H. Cohen, Phys. Rev. B **66**, 214206 (2002).

[18] T. Saha, I. Dasgupta, and A. Mookerjee, J. Phys.: Condens. Matter **6**, L245 (1994).

[19] T. Saha and A. Mookerjee, J. Phys.: Condens. Matter **8**, 2915 (1996).

[20] A. Alam and A. Mookerjee, J. Phys.: Condens. Matter **21**, 195503 (2009); T. Saha, I. Dasgupta, and A. Mookerjee, Phys. Rev. B **50**, 13267 (1994).

[21] A. Alam, S. Ghosh, and A. Mookerjee, Phys. Rev. B **75**, 134202 (2007); A. Alam and A. Mookerjee, *ibid.* **69**, 024205 (2004).

[22] A. Alam and A. Mookerjee, Phys. Rev. B **72**, 214207 (2005); K. Tarafder, A. Chakrabarti, K. K. Saha, and A. Mookerjee, *ibid.* **74**, 144204 (2006).

[23] K. Nomura and A. H. MacDonald, Phys. Rev. Lett. **98**, 076602 (2007).

[24] Y. V. Skrypnyk and V. M. Loktev, Phys. Rev. B **75**, 245401 (2007).

[25] T. O. Wehling, A. V. Balatsky, M. I. Katsnelson, A. I. Lichtenstein, K. Scharnberg, and R. Wiesendanger, Phys. Rev. B **75**, 125425 (2007).

[26] N. M. R. Peres, F. Guinea, and A. H. Castro Neto, Phys. Rev. B **73**, 125411 (2006).

[27] P. Biswas, B. Sanyal, M. Fakhruddin, A. Halder, A. Mookerjee, and M. Ahmed, J. Phys.: Condens. Matter **7**, 8569 (1995).

[28] A. Mookerjee, in *Electronic Structure of Alloys, Surfaces and Clusters*, edited by D. D. Sarma and A. Mookerjee (Taylor Francis, London, 2003).

[29] N. Beer and D. G. Pettifor, in *Electronic Structure of Complex Systems*, edited by P. Phariseau and W. M. Temmerman (Plenum, New York, 1984), p. 769.

[30] Vitor M. Pereira, F. Guinea, J. M. B. Lopes dos Santos, N. M. R. Peres, and A. H. Castro Neto, Phys. Rev. Lett. **96**, 036801 (2006); Vitor M. Pereira, J. M. B. Lopes dos Santos, and A. H. Castro Neto, Phys. Rev. B **77**, 115109 (2008).

[31] B. Sanyal, O. Eriksson, U. Jansson, and H. Grennberg, Phys. Rev. **79**, 113409 (2009).